A 3D Unrolling Framework for Joint Sodium MRI Reconstruction and Concentration Quantification

Yilin Cao[1], Caohui Duan[2], Dinggang Shen[1,3,4], Xin Lou[2(✉)], and Kaicong Sun[1(✉)]

[1] School of Biomedical Engineering & State Key Laboratory of Advanced MedicalMaterials and Devices, ShanghaiTech University, Shanghai 201210, China
sunkc@shanghaitech.edu.cn
[2] Department of Radiology, The First Medical Center, Chinese PLA General Hospital, Beijing 100853, China
louxin@301hospital.com.cn
[3] Shanghai United Imaging Intelligence Co., Ltd., Shanghai 200230, China
[4] Shanghai Clinical Research and Trial Center, Shanghai 201210, China

Abstract. Sodium MRI can non-invasively measure tissue sodium concentration (TSC), a key biomarker for stroke, tumor, cartilage degeneration, and other diseases, but severely suffers from intrinsically low signal-to-noise ratio and long scan times. Existing methods typically perform denoising on conventionally reconstructed images and then conduct TSC quantification separately, leading to oversmooth reconstruction for highly accelerated acquisition and prohibiting end-to-end concentration quantification. To fill this gap, we propose the first deep unrolling framework in sodium MRI, termed SoReCon, that takes gridded radial k-space as input and simultaneously performs sodium MRI reconstruction and TSC quantification. To this end, we for the first time craft a sharpness-enhanced training data tailored to obtaining vendor-style sodium MRI reconstruction, such that the reconstructed image achieves an appearance consistent with the vendor-reconstructed image without requiring any post-processing. Besides, we devise a differentiable concentration mapping module containing B1 inhomogeneity correction, automatic phantom detection, and linear transformation to convert the reconstructed image into a TSC map. Experiments on 107 subjects show that our method outperforms the existing representative methods by 7.19 dB in PSNR for image reconstruction and 2.54 mM in MAE for TSC quantification. Prospective evaluation on three additional subjects demonstrates the feasibility of SoReCon under real-world four-fold acceleration, reducing the primary sodium acquisition time from 15 min to 3.75 min and highlighting its potential for clinical translation.

Keywords: Sodium MRI · Joint reconstruction · Quantitative imaging.

Y. Cao and C. Duan contributed equally to this work.

1 Introduction

Sodium MRI (^{23}Na MRI) enables non-invasive measurement of tissue sodium concentration (TSC), providing information on cellular viability and tissue integrity [1, 2]. Changes in tissue sodium levels often precede structural changes, making sodium MRI a potential quantitative biomarker for early diagnosis and treatment monitoring. However, sodium concentration in tissues is substantially lower than proton concentration, and its gyromagnetic ratio is about 3.8 times lower, yielding only 9.2% of the proton signal at the same field strength [3]. This intrinsically low signal-to-noise ratio (SNR) poses significant challenges for accelerated imaging and accurate quantification [4].

To mitigate the low SNR and long acquisition time of sodium MRI, compressed sensing (CS) and other iterative reconstruction methods have been applied to undersampled non-Cartesian data [5, 6]. However, CS methods often require long reconstruction time [8], and are sensitive to the choice of regularization. Besides, the anatomically guided iterative methods use co-registered proton MRI (^{1}H MRI) as prior information, combined with constraints such as total variation, or joint anatomical and sparsity models to improve noise suppression, edge preservation, and spatial resolution [18–21, 12]. For example, in breast sodium MRI, such structurally guided methods improve image sharpness and reduce partial volume effects, but their TSC accuracy still varies with regularization strength [12]. Furthermore, these methods depend on the availability and accurate registration of a separately acquired proton MRI reference.

Over the past decade, deep learning has substantially improved MRI reconstruction [13, 17, 11]. In sodium MRI, several studies apply convolutional neural networks (CNNs) for denoising [7, 8]. Given the scarcity of large-scale sodium MRI datasets, many studies train models with proton MRI data by simulating sodium MRI characteristics [8, 9]. However, this inherently introduces a domain gap that potentially limits model performance on real-world data due to discrepancies in contrast and noise characteristics between simulated and real-world data [16]. Furthermore, these methods apply denoising as postprocessing on conventionally reconstructed images without accessing undersampled k-space data, leading to error accumulation and hence suboptimal TSC quantification [10].

To address these challenges, we propose the first 3D framework that jointly performs sodium MRI reconstruction and TSC quantification from undersampled radial k-space data. Built on deep unrolling-based reconstruction, our network incorporates a Concentration Mapping Module that corrects B1 inhomogeneities and converts the reconstructed images to TSC maps, enabling end-to-end optimization. The main contributions include: 1) An end-to-end mapping from undersampled k-space to TSC maps; 2) Construction of a sharpness-enhanced training set for sodium MRI reconstruction; 3) Integration of a concentration mapping module and concentration loss into network training to enable direct optimization of the TSC maps; 4) Evaluation on 107 retrospective and 3 prospective subjects, demonstrating a 4× reduction in the primary scan time from 15 min to 3.75 min while preserving reconstruction quality and TSC quantification accuracy.

2 Method

2.1 Problem Formulation and Model Architecture

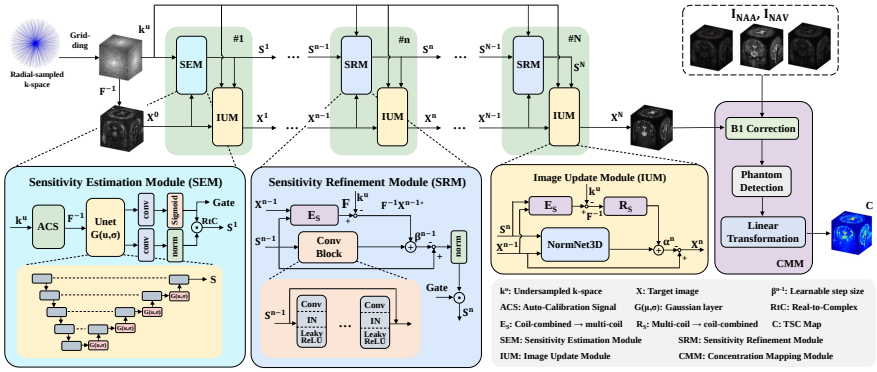

Fig. 1. Architecture of the proposed SoReCon. Top row shows the overall unrolled framework. Bottom row details the architectures of Sensitivity Estimation Module (SEM), Sensitivity Refinement Module (SRM), Image Update Module (IUM), and Concentration Mapping Module (CMM).

In multi-coil MRI, the signal acquired by the m-th coil is modeled as $k_m = \mathcal{F}S_m x + \epsilon_m$, where $x \in \mathbb{C}$ is the complex image, S_m denotes the m-th coil sensitivity map, $\mathcal{F}$ represents the Fourier operator, k_m is the measured k-space data, and ϵ_m denotes the additive noise. For sodium MRI, data is usually acquired with non-Cartesian sampling mask and gridded onto a Cartesian grid, denoted as k_m^u. Inspired by jCAN [11], we establish our SoReCon with $N = 10$ unrolled iterations (Fig. 1). Our SoReCon takes 3D multi-coil undersampled k-space as input and comprises three main components: 1) Sensitivity Estimation Module (SEM) and Sensitivity Refinement Module (SRM) for coil sensitivity map estimation and refinement, 2) Image Update Module (IUM) for image refinement, and 3) Concentration Mapping Module (CMM) for TSC map estimation from the reconstructed magnitude image. The architecture of SEM, SRM, and IUM follow the work of jCAN. More details can be found in [11].

2.2 Construction of Structurally Enhanced Complex-Valued Training Data for Sodium MRI Reconstruction

In Fig. 2, we demonstrate the reconstructed image I_{Grid} using the fully sampled k-space data by the gridding method [27]. We can observe that it exhibits noticeable blurring compared to the vendor-reconstructed image I_{Vendor}. Training a network with I_{Grid} as ground truth would further magnify the oversmoothness,

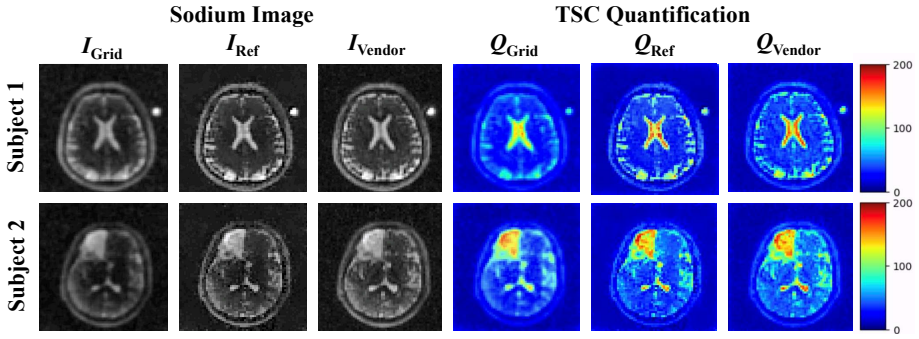

Fig. 2. Validation of I_{Ref} and its TSC map on two subjects. From left to right: gridding reconstruction, structurally enhanced reference image, and vendor reconstruction, together with their corresponding TSC maps.

especially at high acceleration rates. This motivates us to construct a structurally enhanced complex-valued reference I_{Ref} that better preserves structural details.

To obtain I_{Ref}, we introduce an image enhancement pipeline to the fully sampled coil-combined complex-valued image obtained by gridding reconstruction without density compensation. Our pipeline consists of three steps: 1) Wiener deconvolution [14] to compensate for the effective blurring induced by radial sampling density imbalance and gridding interpolation; 2) an edge-aware fusion strategy that selectively integrates the original and deconvolved images based on Laplacian-derived edge maps, thereby suppressing noise amplification while preserving high-frequency structural details, and 3) a second Wiener deconvolution step for further refinement of tissue boundaries and progressive restoration of high-frequency details. Note that all the operations are performed on complex images, ensuring phase consistency throughout the process.

As shown in Fig. 2, the resulting I_{Ref} closely matches the vendor-reconstructed images, achieving an average PSNR of 35.83 ± 1.48 dB across 107 subjects. The corresponding sodium concentration maps Q_{Ref}, derived using the same B1 correction and phantom calibration pipeline as Q_{Vendor}, also show closer agreement with the vendor-estimated counterpart compared to those from I_{Grid}.

2.3 Concentration Mapping Module (CMM)

The CMM converts the final magnitude image into a TSC map through B1 inhomogeneity correction, automatic phantom detection, and linear transformation (Fig. 3). To correct the spatially varying receive sensitivity, four scans are acquired following the dual-mode calibration approach [4, 15] including an NAA mode scan (high SNR, exhibits B1 inhomogeneity), a NAV mode scan (lower SNR, relatively homogeneous), a second NAA mode scan, and the primary sodium scan. The two NAA scans each take approximately 1 min, while

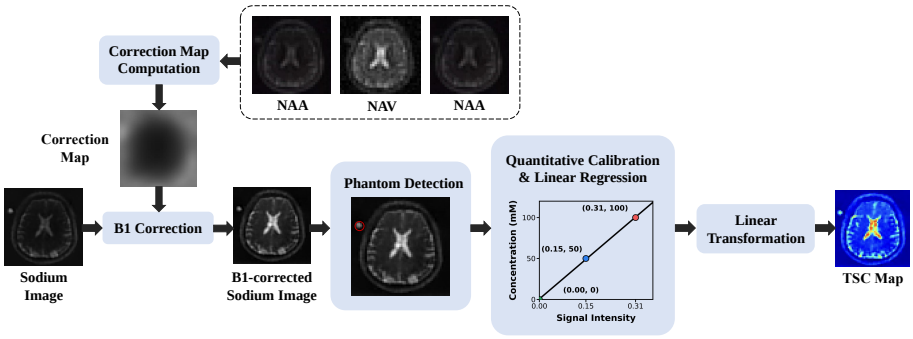

Fig. 3. Pipeline of the Concentration Mapping Module.

the NAV scan takes approximately 6 min, resulting in about 8 min of additional calibration time. All these scans use the same sequence but differ in resolution and coil mode. The two NAA scans are averaged to obtain $\bar{I}_{\mathrm{NAA}}$, and the correction map is computed as $\mathcal{C} = (\bar{I}_{\mathrm{NAA}} + \epsilon)/(I_{\mathrm{NAV}} + \epsilon)$, where $\epsilon = 10.0$ is empirically chosen to prevent noise amplification in low-signal regions. The corrected image is then given by $I_{\mathrm{corrected}} = |x|/\mathcal{C}$.

During sodium MRI acquisition, calibration phantoms (50 mmol/L and 100 mmol/L) are placed around the head as reference standards. To automate signal extraction, we design a phantom detection pipeline operating on axial slices. Specifically, connected components are first identified using 8-connected neighborhood analysis, and each component is characterized by its area A, circularity ρ, and bounding-box aspect ratio R. Components satisfying predefined criteria ($A \in [20, 2000]$, $\rho > 0.7$, $R < 1.7$) are retained and grouped across slices. For each phantom, the representative intensity I is computed as the mean of a $3 \times 3 \times 3$ ROI centered in the middle of the phantom. The resulting intensity–concentration pairs (I, C) for $C = 50$ mmol/L and $C = 100$ mmol/L are used to fit a linear model $C = \alpha I + \beta$ for mapping reconstructed intensity to sodium concentration. When a proportional relationship between sodium concentration and signal intensity is assumed, the model is simplified to the zero-intercept form $\beta = 0$.

2.4 Loss Function

The loss function we used to train SoReCon comprises four components:

$$\mathcal{L} = \sum_{n=1}^{N} w_n \|\mathcal{R}_S(x^n) - I_{\mathrm{Ref}}\|_1 + \lambda_1 \mathcal{L}_{\mathrm{SSIM}}(\mathcal{R}_S(x^N), I_{\mathrm{Ref}}) + \lambda_2 \|\nabla S\|_{2,1} + \lambda_3 \|\hat{Q} - Q_{\mathrm{Ref}}\|_1, \tag{1}$$

where x^N is the final output, and S denotes the set of coil sensitivity maps. The operator $\mathcal{R}_S$ combines multi-coil images into a single complex image. The

isotropic total variation $\|\nabla S\|_{2,1} = \left\| \sqrt{|\nabla_x S|^2 + |\nabla_y S|^2 + |\nabla_z S|^2} \right\|_1$ is adopted to enforce the smoothness of coil sensitivity maps. The final term, i.e., the concentration loss, penalizes the discrepancy between estimated concentration map $\hat{Q}$ and the reference map Q_{Ref}.

3 Experiments and Results

3.1 Dataset and Implementation Details

Our initial dataset includes 110 brain sodium MRI scans (mean age, 46 ± 16 years; range, 8–75 years; 50 females and 60 males). Three cases were excluded during quality control, and the remaining 107 cases were split at the subject level into 77 for training, 10 for validation, and 20 for testing. All the scans were acquired on a 7T MRI scanner (Magnetom Terra, Siemens Healthcare, Erlangen, Germany) using a dual-tuned ^{23}Na/^{1}H head coil (RAPID Biomed GmbH, Rimpar, Germany), consisting of a dual-tuned ^{23}Na/^{1}H quadrature Tx/Rx birdcage coil and 32-channels receive-only ^{23}Na array. A 3D radial projection sequence (7500 fully sampled spokes, 500 radial samples, TR/TE = 120/0.4 ms, flip angle = 90°, field of view = $224 \times 224 \times 224$ mm^3, nominal resolution = $3.5 \times 3.5 \times 3.5$ mm^3) was used for ^{23}Na MRI, with a primary sodium acquisition time of approximately 15 min per scan.

Our model was implemented in PyTorch and trained on an NVIDIA A100 GPU with 40 GB RAM. We used the Adam optimizer with an initial learning rate of 10^{-4} decayed by 0.5 every 30 epochs and the mini-batch size was set as 1. The first 50 epochs used only the reconstruction loss and the remaining 50 epochs integrated the concentration loss. We employed an exponentially decaying schedule $w_n = \gamma^{N-n}$ with $\gamma = 0.85$, assigning higher importance to later blocks. Loss weights were selected as $\lambda_1 = 1$, $\lambda_2 = 100$, and $\lambda_3 = 0.3$ based on the reconstruction performance on the validation set.

3.2 Experimental Results

We compared our method with three representative methods including NUFFT reconstruction [24] incorporating Pipe–Menon density compensation [22], wavelet-based CS [25], and a U-Net reconstruction model [26]. We retrospectively undersampled the reference radial k-space data (7500 spokes) to generate 2× (3,750 spokes) and 4× (1,875 spokes) acceleration.

Quantitative Comparison. Table 1 presents quantitative comparisons of both image reconstruction and TSC quantification. We can see that for 2× and 4× accelerations, our approach achieves the highest PSNR and SSIM for image reconstruction and the lowest MAE for TSC quantification. Notably, although CS achieves higher PSNR and SSIM than NUFFT at 2×, it shows worse TSC quantification performance with a higher MAE, suggesting that image-domain

similarity evaluated by PSNR and SSIM does not necessarily translate into concentration accuracy [23]. Therefore, we additionally evaluate the MAE of TSC quantification and perform visual assessment to assess both reconstruction fidelity and TSC quantification accuracy.

Table 1. Quantitative comparison of image reconstruction and TSC quantification.

Accel.	Method	Image Reconstruction		TSC Quantification
		PSNR (dB)	SSIM	MAE (mM)
2×	NUFFT	29.39 ± 1.46	0.8543 ± 0.0205	7.94 ± 2.63
	CS	35.70 ± 1.08	0.9000 ± 0.0138	8.42 ± 2.54
	U-Net	32.10 ± 1.31	0.9182 ± 0.0169	7.67 ± 2.92
	Ours	**40.16 ± 1.25**	**0.9480 ± 0.0129**	**6.20 ± 3.21**
4×	NUFFT	23.57 ± 1.07	0.6861 ± 0.0315	9.72 ± 3.54
	CS	32.31 ± 1.29	0.8125 ± 0.0274	8.70 ± 2.59
	U-Net	31.72 ± 1.14	0.9000 ± 0.0194	9.34 ± 3.12
	Ours	**39.50 ± 1.24**	**0.9402 ± 0.0118**	**6.16 ± 2.74**

Qualitative Comparison. Fig. 4 shows that our method preserves sharper structural details with less blurring than the compared methods and provides concentration maps closer to the reference ones.

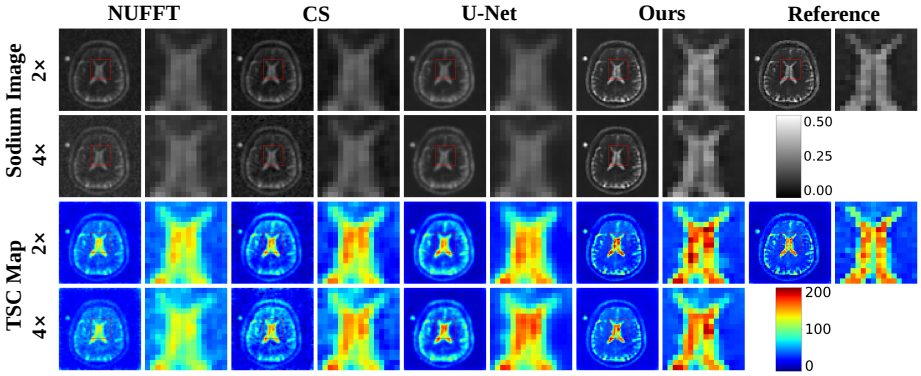

Fig. 4. Visual comparison at 2× and 4× acceleration. Reconstructed images and TSC maps are shown in the top and bottom rows, respectively.

Ablation Study. We illustrate the necessity of CMM by comparing two variants: training without and with CMM. As shown in Table 2, including the concentration loss substantially improves the accuracy of the TSC map. The results indicate that our model achieves an effective balance, delivering both high-quality image reconstruction and concentration quantification.

Table 2. Ablation study on the concentration loss for 2× and 4× acceleration.

Accel.	Setting	Image Reconstruction		TSC Quantification
		PSNR (dB)	SSIM	MAE (mM)
2×	w/o CMM	39.55 ± 1.06	**0.9492 ± 0.0103**	7.79 ± 3.74
	w/ CMM	**40.16 ± 1.25**	0.9480 ± 0.0129	**6.20 ± 3.21**
4×	w/o CMM	**39.93 ± 1.44**	**0.9410 ± 0.0125**	9.17 ± 4.90
	w/ CMM	39.50 ± 1.24	0.9402 ± 0.0118	**6.16 ± 2.74**

Table 3. Prospective evaluation on three subjects for 2× and 4× acceleration.

Accel.	Image Reconstruction		TSC Quantification
	PSNR (dB)	SSIM	MAE (mM)
2×	38.32 ± 0.25	0.9181 ± 0.0071	5.54 ± 2.25
4×	37.76 ± 0.43	0.9137 ± 0.0050	6.24 ± 2.68

Prospective Evaluation. Besides retrospective study, we prospectively evaluated three additional subjects acquired at 2× and 4× acceleration, together with the corresponding reference acquisitions. Table 3 summarizes the reconstruction and TSC quantification performance. We can see that even at 4× acceleration, our model achieves an average PSNR of 37.76 dB and average MAE of 6.24 mM.

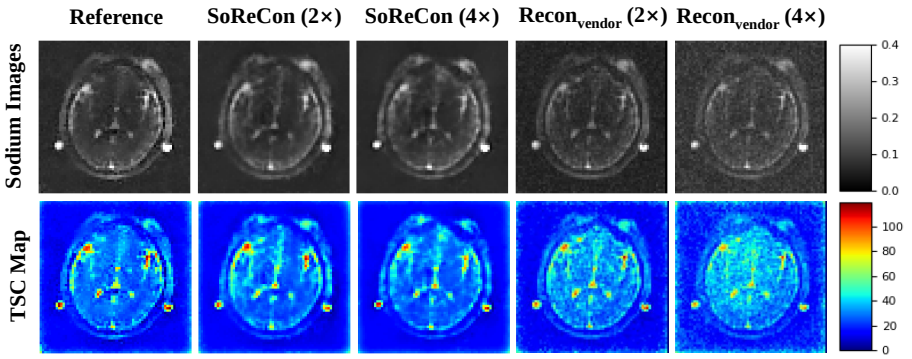

Fig. 5. Prospective results for one representative subject. "Recon$_{vendor}$" denotes the image reconstructed by the vendor's proprietary reconstruction pipeline.

Fig. 5 shows the results for a representative subject. The reconstructed images and the corresponding TSC maps generated by our model exhibit substantially improved agreement with the reference images and consistently outperform the vendor-reconstructed images. These results demonstrate that our method preserves both reconstruction quality and TSC quantification accuracy while reduc-

ing the primary sodium acquisition time from 15 min to 3.75 min. Nevertheless, prospective validation was conducted on only three subjects, and validation in a larger prospective cohort is warranted.

4 Conclusion

In this paper, we presented SoReCon, the first end-to-end 3D deep unrolling framework for joint sodium MRI reconstruction and concentration quantification from undersampled radial k-space data. We first constructed a structurally enhanced complex-valued training set for learning vendor-style sodium MRI reconstruction. To enable joint optimization of image reconstruction and concentration quantification, we propose a differentiable concentration mapping module that consists of B1 inhomogeneity correction, automatic phantom detection, and linear transformation. Experiments show that our method achieves superior performance in both reconstruction fidelity and concentration accuracy over the compared methods for 2× and 4× accelerations. Prospective evaluation on three additional subjects further demonstrates the feasibility of SoReCon under real accelerated acquisition, reducing the primary sodium acquisition time from 15 min to 3.75 min at 4× acceleration while largely preserving both reconstruction fidelity and concentration quantification performance. Our SoReCon opens up new avenues for accelerated sodium MRI and potentially facilitates the integration of accelerated sodium MRI into clinical workflows.

Acknowledgments. This work was supported in part by National Natural Science Foundation of China (grant numbers 82327803, 62301318, U23A20295, 62131015, 82441023), the China Ministry of Science and Technology (STI2030-Major Projects-2022ZD0209000, STI2030-Major Projects-2022ZD0213100), The Key Area Research and Development Program of Guangdong Province (grant number 2023B0303040001), and HPC Platform of ShanghaiTech University.

Disclosure of Interests. The authors have no competing interests to declare that are relevant to the content of this article.

References

1. Thulborn, K., Lui, E., Guntin, J., Jamil, S., Sun, Z., Claiborne, T.C., Atkinson, I.C.: Quantitative sodium MRI of the human brain at 9.4 T provides assessment of tissue sodium concentration and cell volume fraction during normal aging. NMR in Biomedicine **29**(2), 137–143 (2016)
2. Madelin, G., Regatte, R.R.: Biomedical applications of sodium MRI in vivo. Journal of Magnetic Resonance Imaging **38**(3), 511–529 (2013)
3. Zaric, O., Juras, V., Szomolanyi, P., Schreiner, M., Raudner, M., Giraudo, C., Trattnig, S.: Frontiers of Sodium MRI Revisited: From Cartilage to Brain Imaging. Journal of Magnetic Resonance Imaging **54**(1), 58–75 (2021)

4. Lachner, S., Ruck, L., Niesporek, S.C., Utzschneider, M., Lott, J., Hensel, B., Dörfler, A., Uder, M., Nagel, A.M.: Comparison of optimized intensity correction methods for 23Na MRI of the human brain using a 32-channel phased array coil at 7 Tesla. Zeitschrift für Medizinische Physik **30**(2), 104–115 (2019)
5. Blunck, Y., Kolbe, S.C., Moffat, B.A., Ordidge, R.J., Cleary, J.O., Johnston, L.A.: Compressed sensing effects on quantitative analysis of undersampled human brain sodium MRI. Magnetic Resonance in Medicine **83**(3), 1025–1033 (2020)
6. Behl, N.G., Gnahm, C., Bachert, P., Ladd, M.E., Nagel, A.M.: Three-dimensional dictionary-learning reconstruction of 23Na MRI data. Magnetic Resonance in Medicine **75**(4), 1605–1616 (2016)
7. Adlung, A., Paschke, N.K., Kämmerer, S., et al.: 23Na MRI in ischemic stroke: Acquisition time reduction using postprocessing with convolutional neural networks. NMR in Biomedicine **34**(4), e4474 (2021)
8. Baker, R.R., Bangerter, N.K., O'Brien, K., et al.: Rapid 2D 23Na MRI of the calf using a denoising convolutional neural network. Magnetic Resonance Imaging **110**, 184–194 (2024)
9. Raymond, C., Calkins, K.L., Zhang, Y., et al.: Super-resolution sodium MRI of human gliomas at 3T using physics-based generative artificial intelligence. Journal of Neuro-Oncology **174**(3), 653–665 (2025)
10. Feng, X., Zhang, C., Chen, Z., Zhao, B., Liu, Q., Zhu, Y., Zheng, H., Liang, D., Liu, X.: IMJENSE: Scan-specific implicit representation for joint coil sensitivity and image estimation in parallel MRI. IEEE Transactions on Medical Imaging **42**(9), 2676–2688 (2023)
11. Sun, K., Wang, Q., Shen, D.: Joint Cross-Attention Network With Deep Modality Prior for Fast MRI Reconstruction. IEEE Transactions on Medical Imaging **43**(1), 558–569 (2024)
12. Zaric, O., Leser, C., Juras, V., et al.: Improved tissue sodium concentration quantification in breast cancer by reducing partial volume effects: a preliminary study. arXiv preprint arXiv:2503.19570 (2025)
13. Aggarwal, H.K., Mani, M.P., Jacob, M.: MoDL: Model-Based Deep Learning Architecture for Inverse Problems. IEEE Transactions on Medical Imaging **38**(2), 394–405 (2019)
14. Wiener, N.: Extrapolation, Interpolation, and Smoothing of Stationary Time Series. MIT Press, Cambridge (1949)
15. Niesporek, S.C., Hoffmann, S.H., Berger, M.C., Benkhedah, N., Kujawa, A., Bachert, P., Nagel, A.M.: Partial volume correction for in vivo 23Na-MRI data of the human brain. NeuroImage **112**, 353–363 (2015)
16. Knoll, F., Hammernik, K., Zhang, C., Moeller, S., Pock, T., Sodickson, D.K., & Akcakaya, M. (2020). Deep-Learning Methods for Parallel Magnetic Resonance Imaging Reconstruction: A Survey of the Current Approaches, Trends, and Issues. *IEEE Signal Processing Magazine*, *37*(1), 128–140. https://doi.org/10.1109/MSP.2019.2950640
17. Sriram, A., Zbontar, J., Murrell, T., Defazio, A., Zitnick, C.L., Yakubova, N., Knoll, F., Johnson, P.: End-to-End Variational Networks for Accelerated MRI Reconstruction. In: Medical Image Computing and Computer Assisted Intervention – MICCAI 2020. LNCS, vol. 12262, pp. 64–73. Springer, Cham (2020)
18. Gnahm, C., Bock, M., Bachert, P., Semmler, W., Behl, N.G.R., Nagel, A.M.: Iterative 3D projection reconstruction of ^{23}Na data with an ^{1}H MRI constraint. Magnetic Resonance in Medicine **71**(5), 1720–1732 (2014). https://doi.org/10.1002/mrm.24827

19. Gnahm, C., Nagel, A.M.: Anatomically weighted second-order total variation reconstruction of ^{23}Na MRI using prior information from ^{1}H MRI. NeuroImage **105**, 452–461 (2015). https://doi.org/10.1016/j.neuroimage.2014.11.006
20. Lachner, S., Zaric, O., Utzschneider, M., Minarikova, L., Zb'yň, Š., Hensel, B., Trattnig, S., Uder, M., Nagel, A.M.: Compressed sensing reconstruction of 7 Tesla ^{23}Na multi-channel breast data using ^{1}H MRI constraint. Magnetic Resonance Imaging **60**, 145–156 (2019). https://doi.org/10.1016/j.mri.2019.03.024
21. Zhao, Y., Guo, R., Li, Y., Thulborn, K.R., Liang, Z.-P.: High-resolution sodium imaging using anatomical and sparsity constraints for denoising and recovery of novel features. Magnetic Resonance in Medicine **86**(2), 625–636 (2021). https://doi.org/10.1002/mrm.28767
22. Pipe, J.G., Menon, P.: Sampling density compensation in MRI: Rationale and an iterative numerical solution. Magnetic Resonance in Medicine **41**(1), 179–186 (1999)
23. Haldar, J.P.: The "State of the Art" in MR image reconstruction? Knowledge, culture, and what we leave behind in an era of big data and machine learning. Magnetic Resonance in Medicine (2026). https://doi.org/10.1002/mrm.70377
24. Fessler, J.A., Sutton, B.P.: Nonuniform fast Fourier transforms using min-max interpolation. IEEE Transactions on Signal Processing **51**(2), 560–574 (2003).
25. Lustig, M., Donoho, D., Pauly, J.M.: Sparse MRI: The application of compressed sensing for rapid MR imaging. Magnetic Resonance in Medicine **58**(6), 1182–1195 (2007). https://doi.org/10.1002/mrm.21391
26. Ronneberger, O., Fischer, P., Brox, T.: U-Net: Convolutional networks for biomedical image segmentation. In: Navab, N., Hornegger, J., Wells, W.M., Frangi, A.F. (eds.) Medical Image Computing and Computer-Assisted Intervention – MICCAI 2015. LNCS, vol. 9351, pp. 234–241. Springer, Cham (2015). https://doi.org/10.1007/978-3-319-24574-4_28
27. Jackson, J.I., Meyer, C.H., Nishimura, D.G., Macovski, A.: Selection of a convolution function for Fourier inversion using gridding. IEEE Transactions on Medical Imaging **10**(3), 473–478 (1991). https://doi.org/10.1109/42.97598